Effect of Cutting Speed on Surface Integrity and Chip Formation in Micro-cutting of Zr-based Bulk Metallic Glass

Sau Yee Chau[1], Suet To[1, *], Hao Wang[2], Wai Sze Yip[1], Kang Cheung Chan[3], Chi Fai Cheung[1]

[1] State Key Laboratory in Ultraprecision Machining Technology, Department of Industrial and Systems Engineering, The Hong Kong Polytechnic University, Hung Hom, Kowloon, Hong Kong SAR, PR China

[2] Department of Mechanical Engineering, Faculty of Engineering, National University of Singapore, Block EA, #07-08, 9 Engineering Drive 1, 117575, Singapore

[3] Advanced Manufacturing Technology Research Center, Department of Industrial and Systems Engineering, The Hong Kong Polytechnic University, Hung Hom, Kowloon, Hong Kong SAR, PR China

*Corresponding author email: sandy.to@polyu.edu.hk

Abstract

Single-shear plane theory is an effective tool for understanding the cutting mechanisms of conventional and precision machining. This study investigates the formation of multiple shear bands in micro-cutting of zirconium-based bulk metallic glass (BMG) where classic models have not been studied. A series of slip-steps were observed in the cutting direction which was significantly affected by cutting speed. Surface roughness of the machined surface in micro-cutting BMG was found to be sensitive to the cutting speed. Electron microscopy studies further confirmed the mechanism of the micro-cutting-induced nanocrystallization with the formation of shear bands within the primary deformation zone in the micro-cutting process under various cutting speeds. This work contributes to demonstrating the effects of cutting speed on the formation of the shear band and the serrated flow behavior under complex loading and boundary conditions in micro-cutting.

1. Introduction

Single point diamond turning (SPDT) is a representative cutting technique in ultra-precision machining that enables the generation of optical-quality components with submicron form accuracy and nanometer surface roughness using mono-crystal diamond tools [1]. Material behaviors of machined materials in SPDT play important roles in achieving stringent dimensional accuracy and stability of the machined surface due to the micrometer range of cut depths. There have been numerous studies of the cutting mechanism of SPDT of non-ferrous materials, such as copper [2], aluminium [3] and silicon [4]. Other than non-ferrous materials, bulk metallic glasses (BMG) have also been attracted attention from researchers due to their unique properties in comparison to traditional metals. Bulk metallic glasses are alloys with an "amorphous" atomic structure, which results in the absence of crystallites, grain boundaries, and dislocations [5-7]. The amorphous structure provides unique properties including superior mechanical strain and hardness, excellent corrosion, and wear resistance [8], which lead to a potentially wide range of functional and high precision applications. However, BMG is a difficult to machine material due to its low thermal conductivity and high strength [9]. Some research works have been done for studying the machining mechanisms of BMGs to improve its machinability.

Bakkal et al. [10] reported that the cutting temperature in machining Zr-based BMG can reach 2400-2700K, which induced oxidation and crystallization of Zr-based bulk metallic glass. The unique lamellar chips were found in machining of bulk metallic glass. The lamellar chip formation is the integral result of the self-sustained limit-cycle phenomenon in stress, free volume and temperature in the primary shear zone [11]. Chen [12] reported the nano-crystallization phenomenon appeared at the machined surface in the micro-cutting of BMG, and, a mirror surface could not be achieved easily due to its viscous flow, the optimum surface roughness was reported as 100 nm.

The plastic deformation of amorphous alloys is generated due to the formation of highly localized shear bands, which are induced by the serrated plastic flow [13]. The initiation and the propagation of shear bands in Zr-based BMG under quasi-static and dynamic loading in compression have been investigated in depth [14]. Besides, the effect of strain rate on the compressive failure strength was reported to decrease with an increase of strain rate [15]. It was reported in the literature that the plasticity of BMG is enhanced by the formation of multiple shear bands in the process of quasi-static uniaxial compression testing [16]. However, the nature of initiation and propagation of the shear bands of BMG under complex loading and boundary conditions during micro-cutting remains unclear. In addition, the presence of multiple shear bands in micro-cutting cannot be explained by the classical single-shear plane model for the micro-cutting of BMG.

The previous research on the microscopic material removal mechanisms in SPDT mostly focuses on the metallurgical properties and the machinability of crystalline materials, with little attention to the cutting mechanics of diamond turning of amorphous metals such as BMG. Previous studies indicated that surface roughness of a machined surface is sensitive to cutting speed therefore a relatively smooth surface can be obtained with low cutting speed, but no satisfactory explanation has been provided for this phenomenon [17]. The nature of initiation and propagation of the multiple shear bands of BMG under complex loading and boundary conditions during micro-cutting remains unclear. Therefore, the effects of the cutting speeds on the shear band formation and propagation mechanisms in the micro-cutting of BMG have not been fully understood. To address the above issues, the morphological features of the primary deformation zone and their effects on surface roughness in the diamond cutting of Zr-based BMG are investigated experimentally, and the crystallographic changes induced by the micro-cutting process at three different speeds are characterized through

the study of high-resolution transmission electron microscopy (HRTEM) in this study.

2. Experimental procedures

The material used for the experiment was $Zr_{55}Cu_{30}Ni_5Al_{10}$ amorphous alloy. Round bars of $Zr_{55}Cu_{30}Al_{10}Ni_5$ with 5mm in diameter and 70mm in length were prepared in arc melting furnace with copper mold under a high purity argon atmosphere. The amorphous nature of the fabricated BMG was verified by X-ray diffraction (RigakuSmartLab) with Cu-K_α radiation. The orthogonal micro-cutting tests of BMG were performed on a 4-axis ultra-precision machining system (Moore Nanotech 350FG, USA). The experimental setup is shown in Figure 1. The round bar of the BMG was polished into a rectangular prism with 60 mm (length) x 1 mm (wide) x 4 mm (thick), and was mounted on a specially designed fixture for the micro-cutting. A monocrystal diamond tool with a 2-mm flat cutting edge, zero rake angle and 10° clearance angle was used in the straight cutting experiments. The tool moved in the Z direction with constant cutting speeds of 50mm/min, 100mm/min and 400 mm/min and depth of cut 7 µm. The cutting parameters are listed in Table 1.

In the orthogonal micro-cutting test, the workpiece moved in the Z direction and the single point diamond tool was fixed in location. The diamond tool was stopped at the center of the workpiece during orthogonal cutting; the chip was formed and remained attached to the workpiece surface after the tool retreated in the reverse cutting direction. These experiments were performed in a dry cutting condition to protect the chip morphology. In order to obtain the shear bands in the primary deformation zone (PDZ) after micro-cutting, pre-machining was conducted on the surface parallel and perpendicular to the cutting direction by SPDT, which were labeled in Figure 1a.

The serrated chips remained on the machined surface after the cutting process and were observed by scanning electron microscopy (Hitachi Electron Microscope TM3000)

along the normal direction of the side surface in order to examine the shear bands in the PDZ and the chip morphology. 3D micrographs of the PDZ and machined surface at two different cutting speeds were further examined by an atomic force microscope (Park Systems XE-70 AFM). In addition, surface roughness of the machined surface was determined by a 3D optical surface profiler (Zygo Nexview[TM]). A field emission electron microscope (JEOL JEM-2100F STEM) was employed to investigate the microstructure changes in PDZ after micro-cutting processes. As Figure 1b shown, the cross-section specimens of PDZ in the depth direction perpendicular to the machined surface were prepared by a focused ion beam (Quanta 200 3D DualBeam FIB) with surface coating protection by a sputter coater (Bal-tec SCD 005) using tungsten, with a thickness of 2 µm.
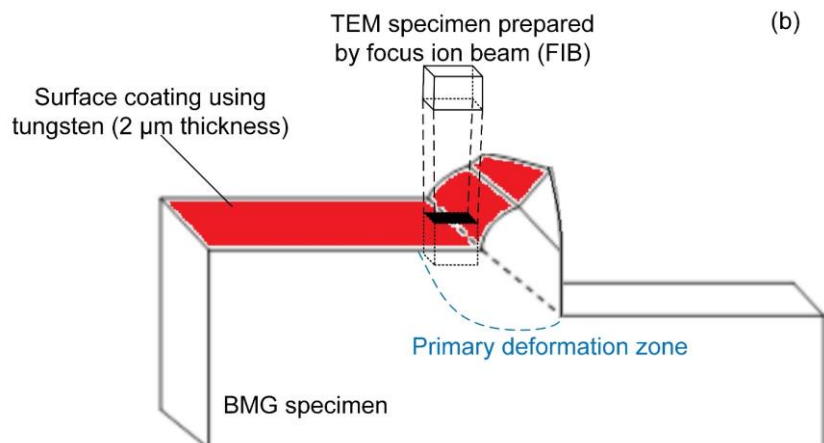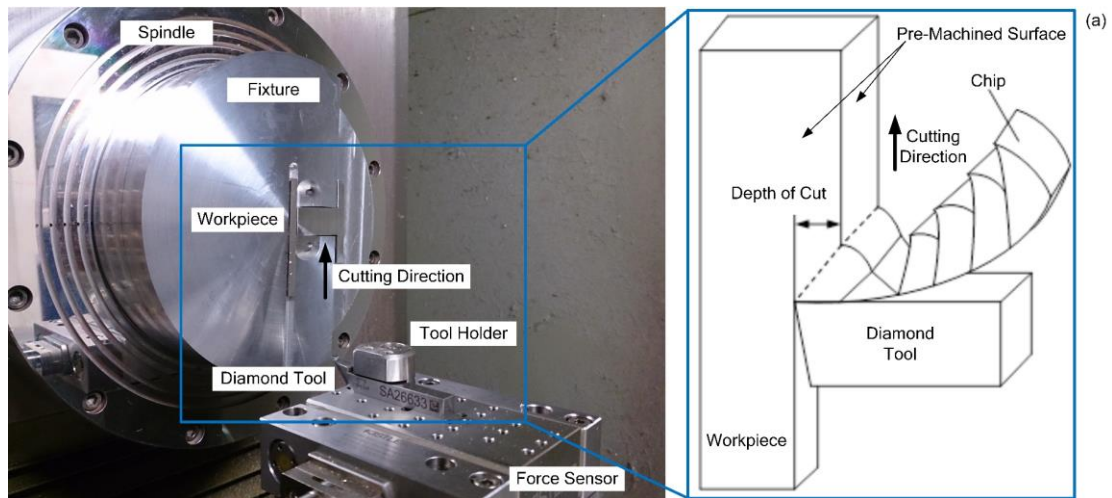
Figure 1. Experimental setup for (a) the straight cutting tests and (b) preparing the cross-section specimens of PDZ by FIB

Table 1 Cutting parameters of orthogonal micro-cutting

| Parameters	Values
Cutting speed (mm/min)	50, 100, 400
Depth of cut (μm)	7
Tool type	Diamond tool
Rake angle of tool (°)	0
Clearance angle of tool (°)	10
Cutting environment	Drying cutting

3. Results and discussion

Figure 2(a) shows a micrograph from scanning electron microscope of a continuous serrated chip generated in the straight cutting of the Zr-based BMG with the diamond tool at 0° under a dry cutting condition. A series of slip-steps due to shear banding emerges along the cutting direction in the PDZ in micro-cutting BMG. The chip morphology in micro-cutting BMG is different from that appearing in crystalline metals, while the slip-steps cannot be obtained in micro-cutting crystalline metal, as shown in Figure 2b [18]. This formation and propagation of shear bands inside the PDZ generally cannot be obtained in machining crystalline materials. The formation of slip-steps revealed that the plastic deformation is highly localized within the PDZ in micro-cutting BMG. The plastic deformation behavior is fundamentally different between metallic glasses and crystalline materials due to the lack of long-range order in metallic glasses. According to the free volume model developed by Spaepen [19], when the external stress is applied and exceeds the activation energy for atomic jumping, the

atoms jump into neighboring holes along the stress direction and create a free volume. With atomic jumping, atomic flow and plastics flow in amorphous metals occur. The increase in stress during micro-cutting promotes slip-steps and accommodates the plastic deformation in the cutting direction. When the accumulated stress reacts or exceeds the yield stress of the work material, it will induce a shear band with a shear angle of 32°. The shear bands are either initiated at the free surface of the cutting specimen and then propagate to the cutting edge of the tool or are initiated at the cutting edge of the tool and then propagate to the free surface in the PDZ, which are shown in the enlarged view (yellow square) in Figure 3 (a). The experimental results indicate that the amorphous alloy experiences deformation behavior in the micro-cutting process.
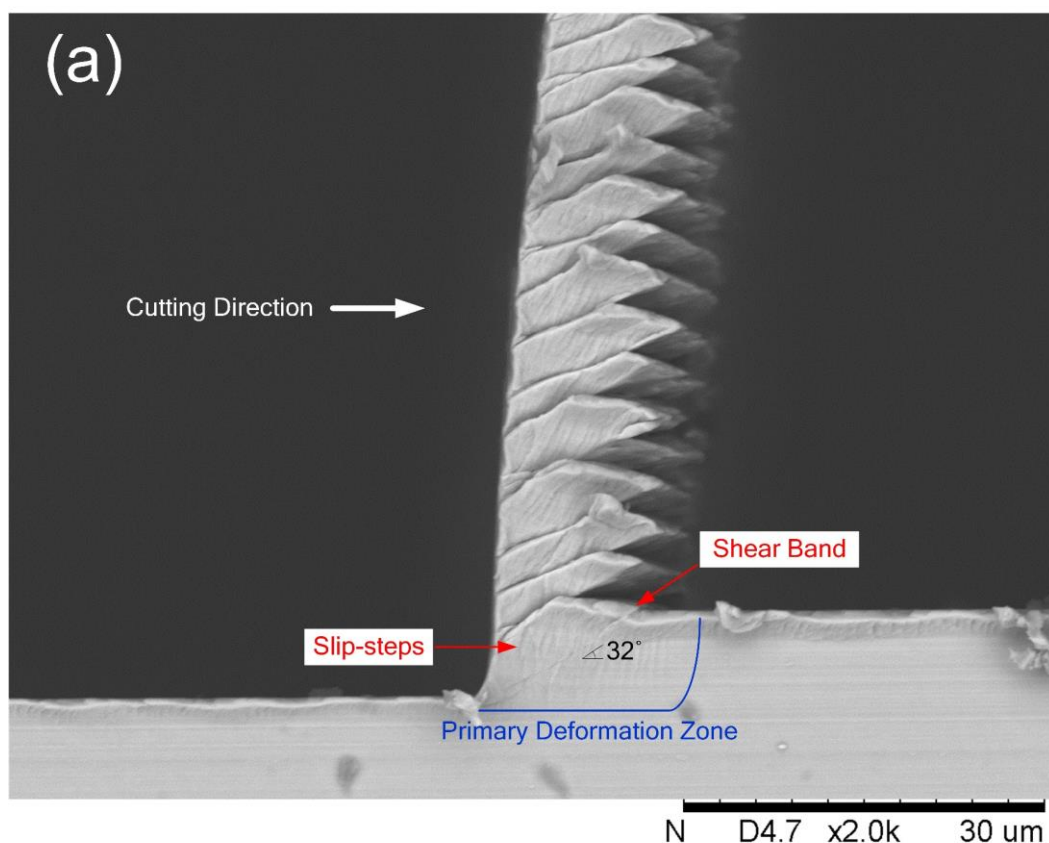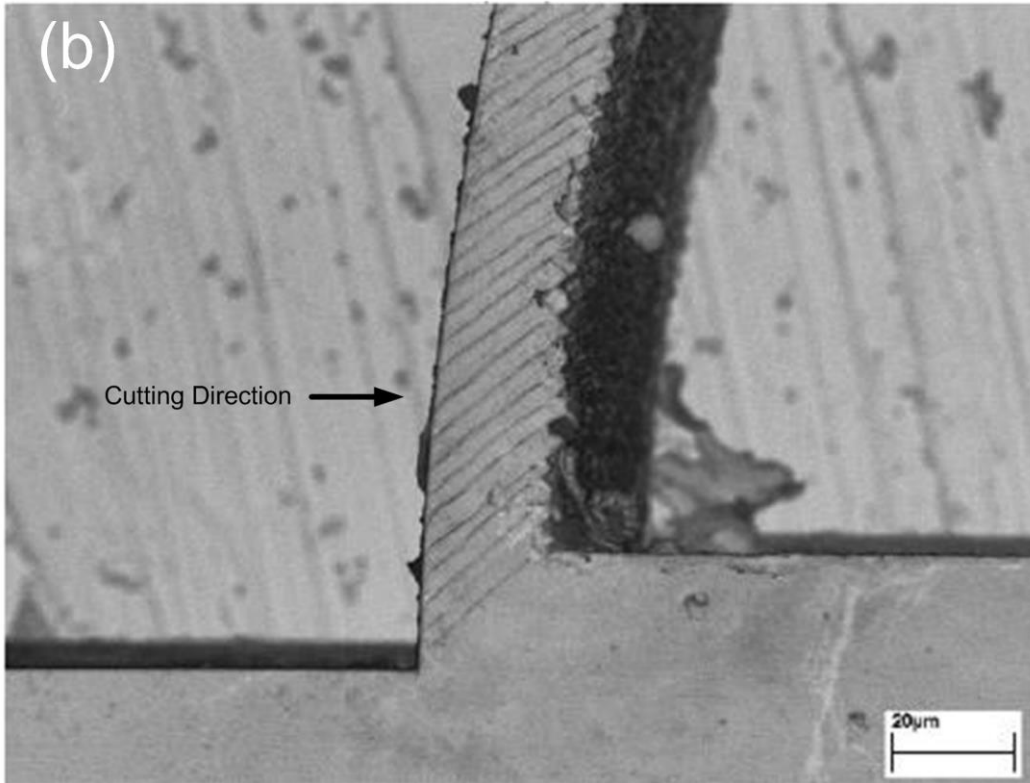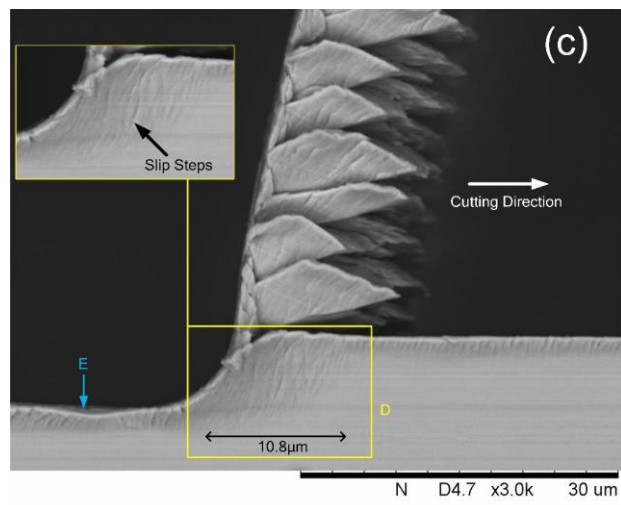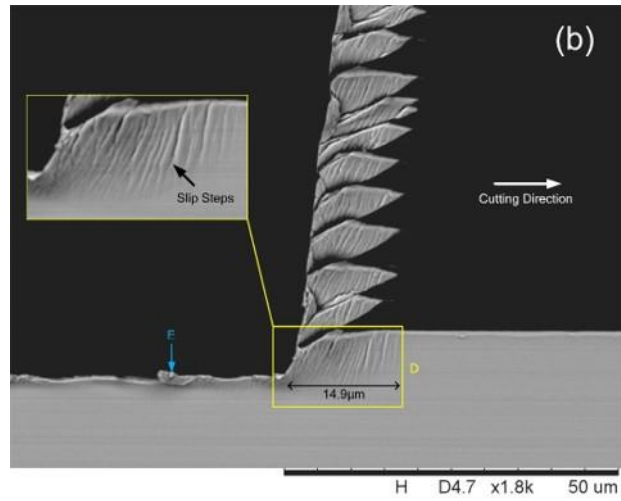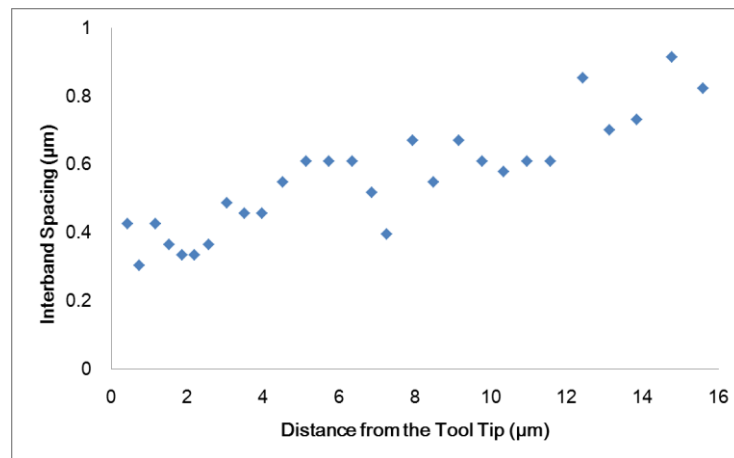
Figure 2. SEM micrograph of chip morphology in micro-cutting (a) Zr-based BMG and (b) cold-rolled brass with a diamond tool at a rake angle of 0°
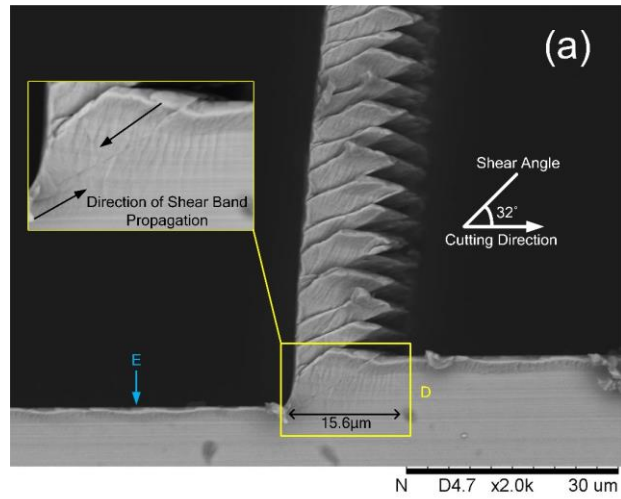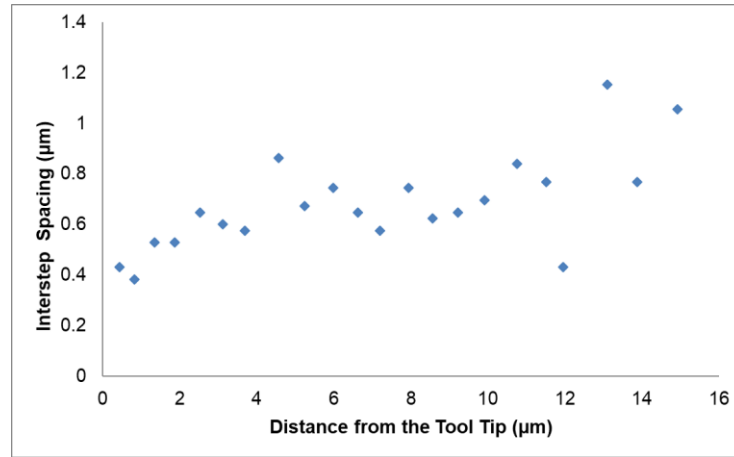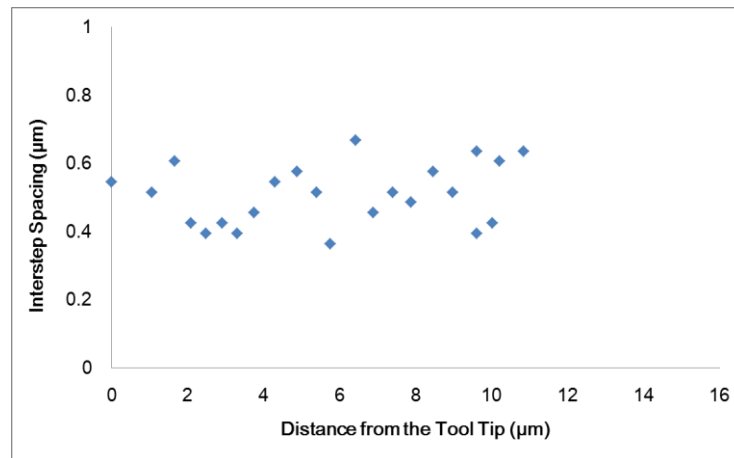
Figure 3. SEM images for primary deformation zone in straight cutting Zr-based BMG with cutting speed at (a) 50 mm/min, (b) 100 mm/min and (c)400mm/min.

(a)

(b)

(c)

Figure 4. Variation of the inter-step spacing as a function of distance from the tool in straight cutting

Zr-based BMG with cutting speed at (a) 50 mm/min, (b) 100 mm/min and (c)400mm/min.

To observe the influences of cutting speed on surface roughness and the chip morphologies, depth of cut was set at 7 µm, with cutting speeds of 50, 100 and 400 mm/min accordingly. Figure 3 shows the morphologies of the PDZ (site D) of the specimen after diamond cutting at the three different cutting speeds. The corresponding chip morphologies and formation of multiple slip-steps at different cutting speeds are visible in the SEM images. Serrated chips were observed at the three different cutting speeds, and the length of the slip-steps in the PDZ and the area of PDZ are shown in Table 2. Figure 4 illustrates the inter-band spacing for the slip-steps formed in the PDZ

as a function of the distance from the cutting tool tip at the cutting speeds of 50 mm/min, 100mm/min and 400 mm/min. For the test at a cutting speed of 50 mm/min and 100mm/min, the inter-step spacing increased when the distance between the tool tip and that inter-step spacing increased. The lowest value of the distance of the inter-step spacing in cutting speed of 50mm/min was 0.3µm and increased to 0.9µm over a distance of 15.6µm. For the test at the cutting speed of 100 mm/min, the lowest value of the inter-step spacing was 0.4µm and increased to 1.2µm over a distance of 14.9µm. For the cutting test at a cutting speed of 400 mm/min, the inter-spacing showed considerable scatter which was consistent with the irregular shapes of the shear band formation. Furthermore, for sample 1, there was a linear increase in spacing with an increase in the distance from the tool tip. It was similar to the observation reported by Xie et al. [20], in which the inter-spacing of the shear bands in $Zr_{41}Ti_{14}Cu_{12.5}Ni_{10}Be_{22.5}$ BMG under Vickers indentation was proportional to the distance from the tip. This result indicates that the formation of primary shear bands in a micro-cutting process is similar to that in the other indentation processes, in which the primary shear bands are firstly initiated at the region around the tool tip and then accommodate the plastic deformation in the cutting direction and appear as slip-steps in PDZ. On the contrary, for sample 3, irregular shapes and scatter spacing of the slip-steps were generated, illustrating the inhabitations of growth and propagation of the slip-steps within a short period by the local stress. However, the present work showed that the total length and the area of PDZ increased significantly by decreasing the cutting speed.

The enlarged view of the PDZ in Figure 3(a) shows that the slip-steps are parallel to each other and fully developed with no intersection at a cutting speed of 50mm/min. Most of the slip-steps remain parallel to each other and fully developed when few irregular slip-steps can be found at a cutting speed of 100 mm/min. When the cutting speed increased from 100mm/min to 400mm/min, more irregular slip-steps aew

generated in PDZ, the slip-steps develop rapidly and irregularly within the PDZ due to the severe plastic deformation. At a low cutting speed, there is sufficient time for the shear bands to release the built-up stresses and avoid crack formation. In contrast, the built-up stresses do not have sufficient time to relax at relativity high cutting speed, which leads to crack formation and a brittle fracture mode. Figure 5 shows the surface topologies and surface roughness of the machined surface. The arithmetic roughness of the machined surface was examined by the 3D optical surface profiler, as shown in Table 2. The arithmetic roughness value, Ra, is the arithmetic average of the absolute values of the profile height deviations from the mean line, recorded within the evaluation length, and can be expressed as equation 1. The Ra values were 13 nm, 25nm and 47 nm at the cutting speeds of 50, 100mm/min and 400 mm/min respectively. The Ra values were increased with increasing in the cutting speed.
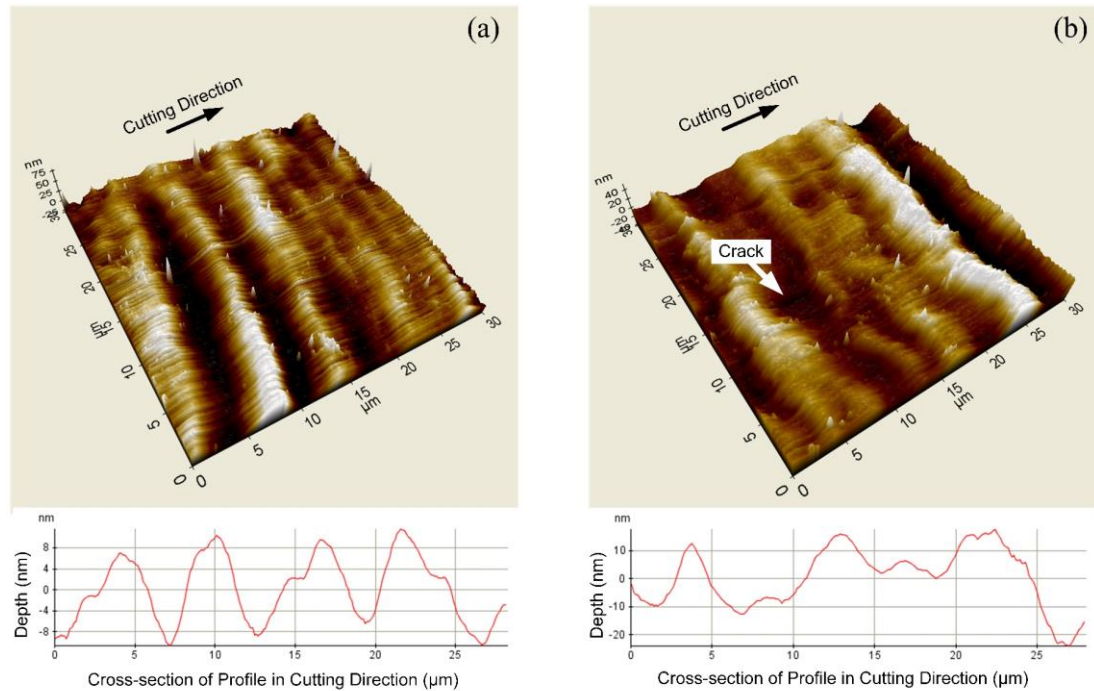
$$R_a = (1/L) \int_0^L |y - y_m| dL \quad (1)$$

where L is evaluation length, y is the profile height and y_m is the height of the mean line.
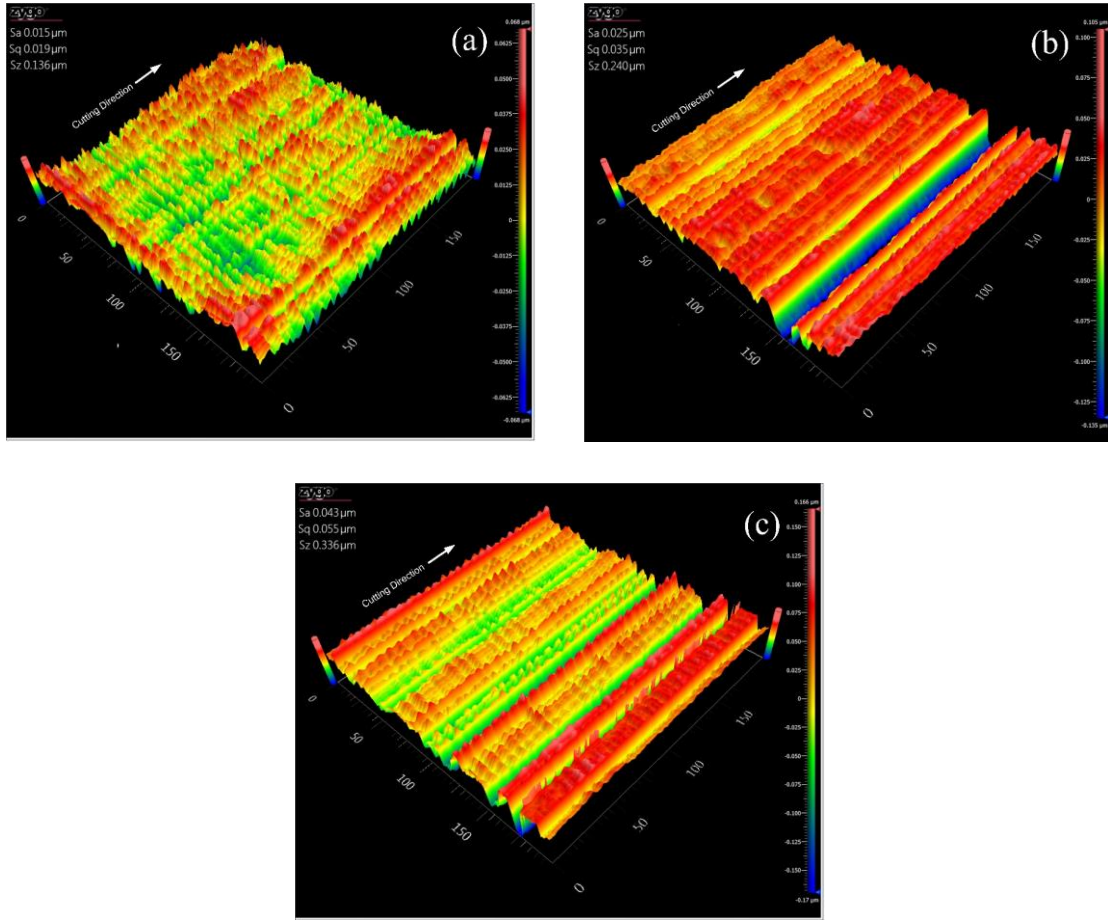
Figure 5. Surface topologies of Zr-based BMG after straight cutting (site E) in cutting speed (a)50 mm/min, (b) 100 mm/min and (c) 400 mm/min

Table 2. Summary of shear bands transformation distance and interval

Sample ID	Cutting speed (mm/min)	Arithmetic roughness Ra (nm)	Length of primary deformtion zone (µm)	Area of primary deformtion zone (µm²)	Number of slip-step
1	50	15	15.6	127.3	28
2	100	25	14.9	113.6	23
3	400	43	10.8	95.8	23

Figure 6. AFM images of machined surface of Zr-based BMG after straight cutting (site E) in cutting speed at (a)50 mm/min and (b) 400 mm/min

In order to compare the effect of different cutting speeds on the machined surface under different cutting speeds, the machined surface of the higher and lower cutting speeds (400mm/min and 50mm/min) in this study are examined by an AFM. The scan size was set at 30µm × 30µm, and the result is shown in Figure 6. The AFM images in Figure 6(b) show the morphologies of the machined surface, in which scratches were found on the machined surface due to the crack formation. The cross-sectional profiles show that the maximum peak to valley height value of sample 1 is about 23nm while the maximum peak to valley height value of sample 3 is over 35nm. The AFM results show that the depth and the period of the grooves in the diamond-turned BMG sample 1 were more regular than those in sample 3. The high loading rate in the micro-cutting process cannot provide sufficient time for the slip steps nucleation and propagation, and the plastic strain is unable to release by the formation of the slip step, the number of slip steps and the total length of the PDZ is decreased by increasing cutting speed. Irregular

slip-steps can be found in PDZ due to the severe plastic deformation in a higher cutting speed. The irregular shapes and scatter spacing of the slip-steps in the cutting speed 400mm/min inhibit the shear band propagation in PDZ, which generates a non-linear shear bad propagation in micro-cutting BMG. This non-linear shear band propagation leads to an irregular geometry shape that extends from the primary deformation zone to the area under the tool tip. Irregular and unpredictable profiles of the machined surface resulted in high-speed micro-cutting. The results suggest that the periodic grooves on the machined surface are associated with the serrated chips with regular slip-steps spacing, the formation of regular shear bands supports the redistribution of the plastic strain and the prevention of crack formation.

The microstructural feature at the PDZ was analyzed by TEM. Figure 7 (a) and (b) show the cross-sectional transmission electron microscopy (XTEM) images and selected area diffraction (SAD) patterns of the PDZ in sample 1 and sample 3 respectively. A homogenous maze contrast was observed, and no crystalline structure could be seen in Figure 7(a). In Figure 7(b), the XTEM image and the SAD pattern revealed that the precipitations of nanocrystalline practices with an average size of 10-15 nm were randomly distributed within the PDZ. In contrast, Figure 7(c) shows the high-resolution transmission electron microscopy (HRTEM) image of machined sample 1 containing shear bands (region 2), where the PDZ (region 1) and the selected area diffraction patterns indicate that the nanocrystals only grow inside the shear bands at low cutting speed, with an average size 3-4 nm. The local heating accompanies the severe localization of plastic flow to the shear bands in the Zr-based metallic glass during deformation, which generates a temperature change from 278 K to more than 1273 K [21]. According to the molecular dynamic simulation, an increase of temperature in the shear bands of CuZr metallic glass is correlated positively with the strain rate under tensile loading [22]. However, the molecular dynamic simulation results showed that

the cutting temperature of Zr-$_{50}$Cu$_{30}$ metallic glasses can reach 600-700K in the nanoscale cutting process [23]. During the deformation process, the temperature was raised by localized adiabatic heating inside the shear bands, playing a crucial role in the nanocrystallization process [24-25]. The temperature of the PDZ in the micro-cutting BMG could reach or exceed the transition temperature (T_g) due to the low thermal conductivity of the Zr$_{55}$Cu$_{30}$Ni$_5$Al$_{10}$ BMG, while the T_g of the Zr$_{55}$Cu$_{30}$Ni$_5$Al$_{10}$ BMG was 673K [26]. Thus, the nanocrystallization process is enabled to occur at the PDZ in the micro-cutting process.
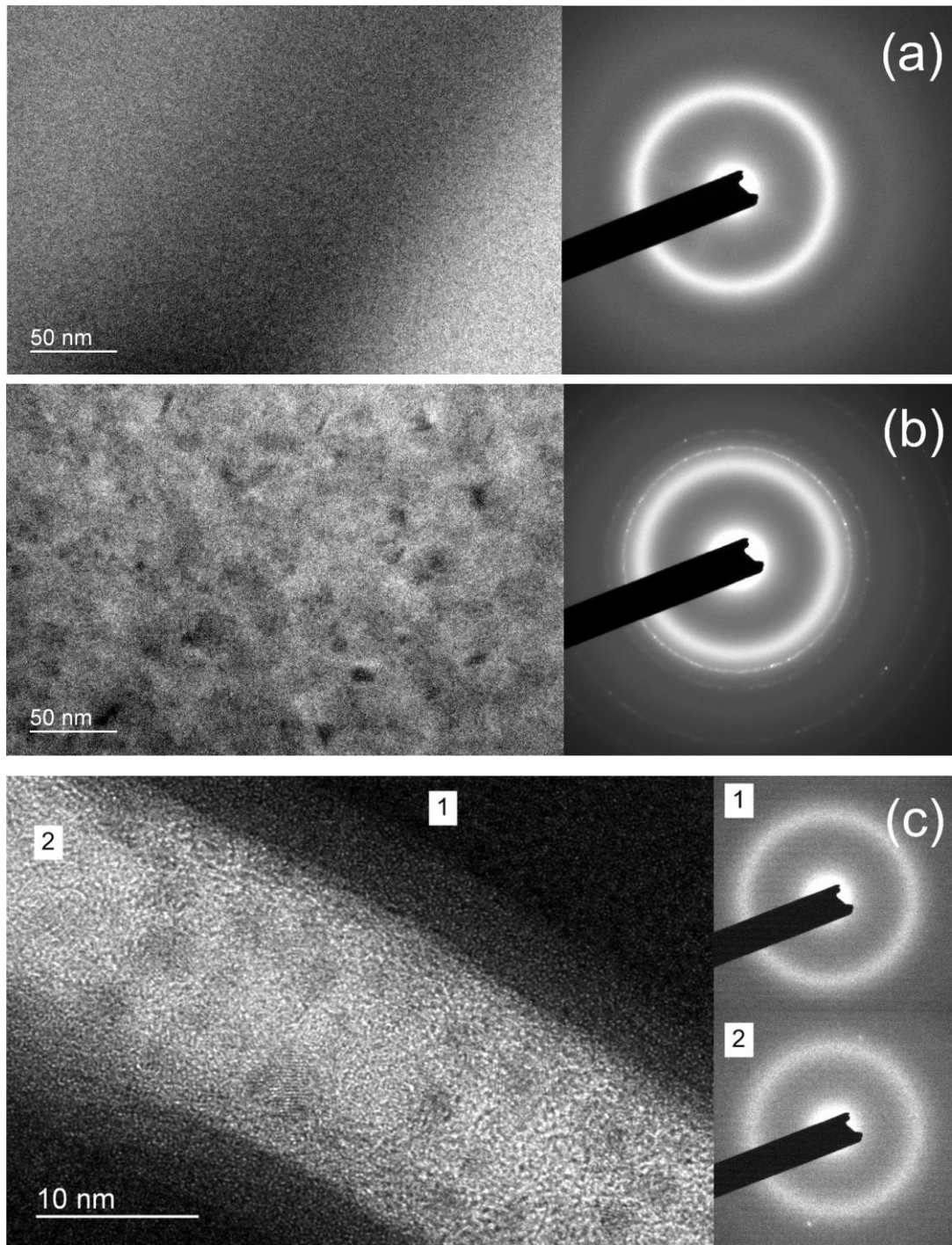
Figure 7. Cross-sectional transmission electron microscopy (XTEM) image of primary deformation zone (PDZ) in (a) sample 1 and (b) sample 2; (c) HRTEM image and selected area diffraction patterns of the shear bands formed in sample 1

Figure 8 shows the mechanism of the formation of nanocrystalline practices with the propagation of primary and secondary shear bands within the PDZ in a micro-cutting process under various cutting speeds. It is noticeable that the shear band initiation and

propagation of the micro-cutting process are highly related to the cutting speed. In the initial stage, a part of local stress would be released by the formation of slip-steps along the cutting direction (Figure 8(a) and (c)). Once the remaining local stress accumulated to the yield point, the shear band would be initialized and propagated in the PDZ with the localized viscous flow. The results from the SEM images indicate that a relatively low speed in micro-cutting would benefit the formation of shear bands, because of a slight increase in the local stress at relatively low cutting speeds in micro-cutting, the local stress could be released by the full development of the slip-steps before the shear bands were initiated. At a lower cutting speed in micro-cutting BMG, it provided sufficient time to nucleate new slip steps from the tool tip to the cutting direction, and the fully developed slip steps could be observed at a larger PDZ area. The shear bands were rapidly initiated to accommodate the large inelastic strain due to a high rate of energy input. The number of slip steps and the PDZ area was relatively smaller in highspeed cutting since the slip-steps in PDZ cannot be fully developed before the shear band initiation. With an increase in the cutting speed, the time for conducting the heat generated by cutting is reduced, and the temperature in the PDZ rises rapidly. The high rate of loading inhibits the formation of slip-steps which generates more amount of heat and thereby raises the temperature in the PDZ due to the low thermal conductivity of BMG. The presence of nanocrystals outside the shear bands at the higher cutting speed indicated that the large shear strain at high rate loading affects the amorphous matrix. Hence, the machining-induced nanocrystallization process is influenced by the cutting speed in micro-cutting BMGs.

By the precipitation of nanocrystals outside the shear bands at high-speed cutting, the propagation of the shear band is suppressed by the nanocrystaline practices. Then, a new shear band would be initiated at an area near the previous corresponding shear band which was stopped by the nanocrystalline practice. As illustrated in Figure 8(d),

the shear bands are propagated in a non-linear way due to the random distribution of nanocrystaline practices in the PDZ. This non-linear shear band propagation leads to an irregular and unpredictable profile of the machined surface in high-speed micro-cutting, as shown in Figure 6(b).

Furthermore, the elastic strain energy in the cutting direction can be absorbed by the formation of slip-steps at low cutting speed. Conversely, the high load rate does not provide sufficient time for the formation of slip-steps; thus, the elastic strain energy in the PDZ leads to material recovery in the region between the tool tip and the material. Multiple intersecting residual shear bands in the form of wrinkles and microcracks can be observed on the machined surface in high-speed cutting, as shown in Figure 6(b), which was a result of the high elastic energy stored in the PDZ. Therefore, a smoother surface with regular grooving can be obtained at a low cutting speed. This result also implies that the high loading rate in micro-cutting of BMG enhances the formation of nanocrystals on the machined BMG surface.
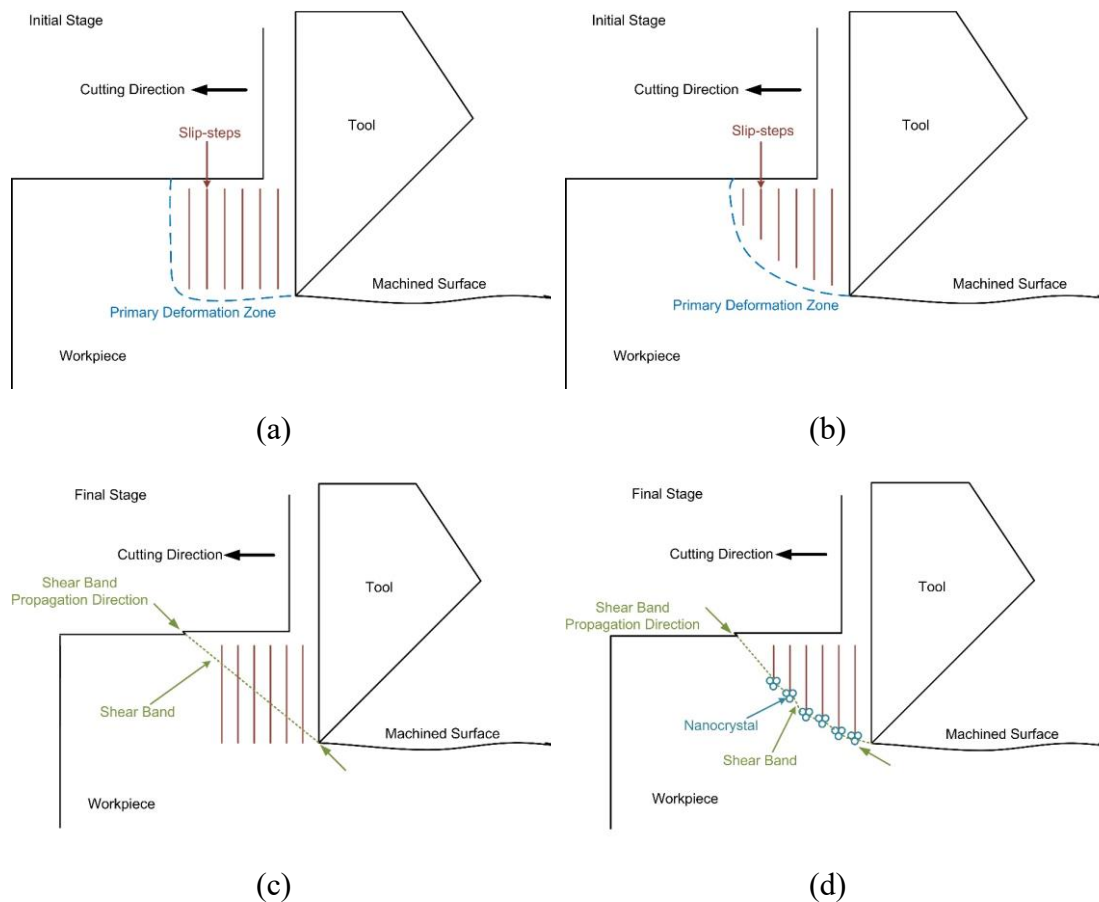
Figure 8. Graphical illustration of formation and propagation of shear band in micro-cutting Zr-based BMG. (a) and (c): The formation and propagation of primary shear bands at an initial stage. (b) and (d): The formation and propagation of secondary shear bands at the final stage. Note the for (a) and (b): cutting speed 50 mm/min, and for (c) and (d): cutting speed 400 mm/min

4. Conclusions

This study investigated the formation of multiple shear bands in the micro-cutting of a Zr-based BMG at three cutting speeds, the following important conclusions are made:

1. Continuous serrated chips appear in diamond straight cutting of the Zr-based BMG.

2. When observing the serrated chips, a series of slip-steps could be seen in the cutting direction at the PDZ and within the serration, while the slip-steps cannot be obtained in micro-cutting crystalline metal.

3. The effects of the cutting speeds on the shear bands formation and propagation mechanisms in micro-cutting of BMG have been observed. The observations

showed that the formation and propagation of shear bands in micro-cutting of BMG are influenced by cutting speed, a higher cutting speed inhibits the growth and propagation of shear bands in the PDZ.

4. The effects of shear band formation and propagation on the machined surface quality have been studied. A finer machined surface is associated with the serrated chips with regular slip-steps spacing, the formation of regular shear bands supports the redistribution of the plastic strain and the prevention of crack formation.

5. Nanocrystals were found inside the shear band at the cutting speed 50mm/min, while nanocrystals were seen outside the shear bands at the cutting speed 400mm/min. The mechanism of the formation and propagation of shear bands in micro-cutting Zr-based BMG, under various cutting speeds, was revealed.

Number G-YBLE).

Conflict of interest The authors declare that there are no conflicts of interest

Ethical approval This work does not contain any ethical issues or personal information

Consent to participate No human or animal was involved in this work;

thus, no consent was required

Consent to publish All authors have given their permission for publishing this work.

References

1.   Ikawa N, Donaldson RR, Komanduri R, König W, Aachen TH, McKeown PA, Moriwaki T, Stowers IF (1991) Ultraprecision metal cutting - the past, the present and the future. CIRP Ann 40(2):587–594.

2.   Moriwaki T, Shamoto E (1991) Ultraprecision diamond turning of stainless steel by applying ultrasonic vibration. CIRP Ann Technol 40(1):559–562.

3.   Sugano T, Takeuchi K, Goto T, Yoshida Y, Ikawa N (1987) Diamond turning of an aluminum alloy for mirror. CIRP Ann 36(1):17–20.

4.   Nakasuji T, Kodera S, Hara S, Matsunaga H, Ikawa N, Shimada S (1990) Diamond turning of brittle materials for optical components. CIRP Ann 39(1):89–92.

5.   Sun BA, Wang WH (2015) The fracture of bulk metallic glasses. Prog Mater Sci 74:211-307.

6.   Ding S, Liu Y, Li Y, Liu Z, Sohn S, Walker FJ, Schroers J (2014) Combinatorial development of bulk metallic glasses. Nat Mater 13:494-500.

7.   Shen Y, Li Y, Chen C, Tsai HL (2017) 3D printing of large, complex metallic glass structures. Mater Des 117:213-222.

8.   Bakkal M, Shih AJ, Scattergood RO (2004) Chip formation, cutting forces, and tool wear in turning of Zr-based bulk metallic glass, Int J Mach Tool Manu 44 (9) 915–925.

9.   Bakkal M, Shih AJ, Scattergood RO, Liu CT (2004) Machining of a Zr–Ti–Al–Cu–Ni metallic glass. Scr Mater 50(5):583–588.

10   Bakkal M, Liu CT, Watkins TR, Scattergood RO, Shih AJ (2004) Oxidation and crystallization of Zr-based bulk metallic glass due to machining Intermetallics 12(2): 195–204.

11   Jiang M, Dai L (2009)   Formation mechanism of lamellar chips during machining of bulk metallic glass. Acta Mater 57(9):2730–2738.

12   Chen X, Xiao J, Zhu Y, Tian R, Shu X, Xu J (2017) Micro-machinability of bulk metallic glass in UPMC. Mater Des 136:1–12.

13.   Chen H S (1973) Plastic flow in metallic glasses under compression. Scr Metall 7(9):931–935.

14.   Liu L F, Dai L H, Bai Y L, Wei BC, Eckert J (2005) Behavior of multiple shear bands in Zr-based bulk metallic glass. Mater Chem Phys 93(1):174–177.

15.   Li H, Subhash G, Gao XL, Kecskes LJ, Dowding RJ (2003) Negative strain rate sensitivity and compositional dependence of fracture strength in Zr/Hf based bulk metallic glasses. Scr Mater 49(11):1087–1092.

16.   Liu LF, Dai LH, Bai YL, Wei BC (2005) Initiation and propagation of shear bands in Zr-based bulk metallic glass under quasi-static and dynamic shear loadings. J Non Cryst Solids 351(40-42):3259–3270.

17. Chau SY, To S, Chan KC, Cheung CF (2014) Cutting characteristics of zirconium based bulk metallic glasses in ultra-precision diamond turning. In: proceedings of the 4th International Conference on Nanomanuufacturing, Bremen, Gemary.

18. Wang H, To S, Chan CY, Cheung CF, Lee WB (2010) A study of regularly spaced shear bands and morphology of serrated chip formation in microcutting process. Scr Mater 63(2):227–230.

19. Spaepen F (1977) A microscopic mechanism for steady state inhomogeneous flow in metallic glasses. Acta Mater 25(4):407–415

20. Xie H, Lin J, Li Y, Yan W, Hodgson P, Wen C (2008) Plastic deformation in Zr41Ti14Cu12.5Ni10Be22.5 bulk metal glass under Vickers indenter. J Alloys Compd 461(1-2):173–177.

21 Thurnheer P, Haag F, Löffler JF (2016) Time-resolved measurement of shear-band temperature during serrated flow in a Zr-based metallic glass. Acta Mater. 115:468-474

22 Tang C, Yi J , Xu W, Ferry M. (2018) Temperature rise in shear bands in a simulated metallic glass. Phys Rev B 98(22):224203-224208.

23. Zhu PZ, Qiu C, Fang FZ, Yuan DD, Shen XC (2014) Molecular dynamics simulations of nanometric cutting mechanisms of amorphous alloy. Appl Surf Sci 317(30):432–442.

24. Lewandowski J, Greer A (2006) Temperature rise at shear bands in metallic glasses. Nature Mater 5(1):15-18.

25. Kim J.J, Choi Y, Suresh S, Argon AS (2002) Nanocrystallization during nanoindentation of a bulk amorphous metal alloy at room temperature. Science 295(5555):654-657.

26. Vaillant ML, Keryvin V, Rouxel T, Kawamura Y (2002) Changes in the mechanical properties of a $Zr_{55}Cu_{30}Al_{10}Ni_5$ bulk metallic glass due to heat treatments below 540 C. Scr Mater 47(1):19-23.